Journal of the European Ceramic Society 44 (2024) 6607–6619

Contents lists available at ScienceDirect

Journal of the European Ceramic Society

journal homepage: www.elsevier.com/locate/jeurceramsoc

Generation of protective ceramic coatings on magnesium by laser treatment of Al_2O_3/ZrO_2 filled organosilazane

Alexander Horcher [a], Katja Tangermann-Gerk [b], Walter Krenkel [a], Michael Schmidt [b], Stefan Schafföner [a], Günter Motz [a,*]

[a] University of Bayreuth, Chair of Ceramic Materials Engineering (CME), Prof.-Rüdiger-Bormann-Straße 1, Bayreuth 95447, Germany
[b] Bayerisches Laserzentrum GmbH, Konrad-Zuse-Straße 2-6, Erlangen 91052, Germany

ARTICLE INFO

Keywords:
Laser pyrolysis
Protective ceramic coatings
Magnesium substrate
Mechanical
Properties
Adhesion

ABSTRACT

Protective ceramic coatings are frequently the most common solutions for problems like corrosion and wear. Polymer derived ceramics technology is suitable for the preparation of ceramic coatings by pyrolysis in a furnace but requires high temperatures for the ceramization. To overcome this restriction a Nd:YVO_4 laser ($\lambda = 1064$ nm) as energy source was used to process a novel ceramic coating system composed of an organosilazane with zirconia and alumina particles specially to protect magnesium. The resulting dense ceramic coating with a thickness up to 20 μm exhibits very good adhesion (25.9 ± 2.7 MPa) to the magnesium substrate, exceptionally high hardness (19.79 ± 1.90 GPa), an outstanding thermal shock stability but also a low coefficient of friction (0.21 ± 0.02) and a very good wear protection towards a SiC counter body. Furthermore, the coating protects the magnesium substrate effectively against corrosion (5 wt% aqueous NaCl solution).

1. Introduction

Low-density materials are key components to realize the goals of climate protection. Thus, for example in the field of transport industry, they can help to increase the fuel efficiency and range, reduce climate-damaging emissions, and allows larger payloads. Magnesium is a low-density material with a specific high strength to weight ratio. With a density of $\rho = 1.7$ g/cm^3 it is 35 % lighter than aluminum ($\rho = 2.7$ g/cm^3) [1,2]. As a structural material with a high strength-to-weight ratio magnesium alloys are especially attractive for applications in the field of next generation automobiles and aerospace components [3]. Despite the positive properties of magnesium alloys, the low wear and corrosion resistance in particular limit their use [3–6]. Therefore, surface treatments and coatings are the most effective methods to increase the corrosion and wear resistance. Several different coating systems and methods have been developed specially to protect magnesium alloys, each of which has specific advantages and disadvantages, for example electrochemical plating and electroplating or coatings, produced by chromating [5,7]. A major disadvantage of these processes is the toxicity of the used chemicals [5,7]. Another coating method is anodizing. By anodizing, hard oxide ceramic like surfaces can be produced. However, theses layers are porous and do not provide sufficient corrosion protection [5,7]. Organic coatings are also commonly used for corrosion protection and for sealing porous layers, but they are limited in the application temperature, susceptible to mechanical damage and do not guarantee sufficient wear protection.

However, to provide simultaneously wear and corrosion protection, ceramic coatings are the best option. Different protective ceramic coating systems for magnesium alloys already exists. Ceramic coatings are especially applied by thermal spraying, physical vapor deposition (PVD) or chemical vapor deposition (CVD). These methods are cost-intensive and have some limitations (e.g., complex vacuum process, high temperature load, reactive gases, low application rates). An alternative technology for the generation of ceramic coatings is the PDC-technology (polymer derived ceramics) [8–15]. Preceramic polymers (precursors) are organometallic compounds, which are mainly based on silicon with additional elements, like carbon, nitrogen, oxygen or even metals in the backbone. The best-known representatives of preceramic polymers are the oxygen-containing polysiloxanes and the non-oxidic polysilanes, polycarbosilanes and polysilazanes [14,16]. Usually, the preceramic polymers are converted into an amorphous ceramic by a thermal treatment between 500 °C and 1000 °C [9]. An advantage of the PDC-technology especially for the processing of coatings is that respective suspensions can be applied to the substrates by simple

* Corresponding author.
E-mail address: guenter.motz@uni-bayreuth.de (G. Motz).

https://doi.org/10.1016/j.jeurceramsoc.2024.04.054
Received 19 December 2023; Received in revised form 21 March 2024; Accepted 21 April 2024
Available online 23 April 2024

methods such as dipping, spraying, spin-coating or by doctor blade [12]. However, one drawback of the PDC route is the high shrinkage of the polymers during pyrolysis, which exceeds 50 % by volume [17]. The shrinkage leads usually to the formation of pores and cracks with increasing layer thickness due to the release of gaseous pyrolysis products. One approach to limit the shrinkage is the use of active and/or passive fillers [11]. In addition to compensating shrinkage, fillers can also be used for purposive adjustment of the coating properties, such as increasing the hardness and to improve the corrosion and abrasion resistance. Especially ceramic fillers are suitable to improve these properties. However, to transform the preceramic polymer-based coatings into ceramics a heat treatment in a furnace at temperatures higher than 800 °C is necessary. Therefore, high-temperature stable substrates like steels, superbase alloys or ceramics are required. Nevertheless, the thermal treatment of the mentioned metallic substrates often leads to a decrease in the mechanical properties due to recrystallization effects [18]. To overcome this issue a laser can be used to generate the required thermal energy. The focusing ability of the laser beam allows the deposition of a defined amount of heat energy to ensure ceramization of the polymer-based coating without thermally effecting the substrate in the best case [19]. Due to the high thermal conductivity of metals in particular, the introduced heat can quickly dissipate laterally. Moreover, as the size of the laser focus diameter is very small in comparison to the substrate dimensions, the heat is also distributed over a large volume. Furthermore, since in laser pyrolysis only a small volume is thermally affected, coatings with low residual stress of the substrate can be generated [19]. Various studies described the interaction between laser radiation and preceramic precursors, whereby the influence of different laser parameters such as wave length, pulse frequency, pulse duration and pulse energy on the pyrolysis behavior as a function of the precursor systems were investigated [19–22]. Other studies already demonstrated that laser pyrolysis is a very suitable approach for the generation of polysilazane-based corrosion and wear protection ceramic coatings on aluminum [23] and stainless steel [24–26].

The key challenge of this study was the development of the laser pyrolysis of a specially designed protective ceramic coating based on silazanes and high melting ceramic fillers on low-melting magnesium substrates. Because of the low melting temperature of magnesium (650 °C) a furnace based pyrolysis of such coatings on magnesium substrates is in general not possible. The laser based pyrolysis provides the unique opportunity to generate thick, hard and dense ceramic coatings on low-melting magnesium substrates. A Nd:YVO_4 laser was used for the laser pyrolysis of the coatings, whereby the absorption behavior of the green coating was adjusted to the wavelength of the laser ($\lambda = 1064$ nm) to successfully convert the organosilazane into a ceramic and to melt the fillers to obtain a pore-free ceramic composite coating. Two commercially available silazanes Durazane 1800 (for the top coat) and Durazane 2250 (for the bond coat) were selected as starting materials due to their good availability, their excellent adhesion to metallic substrates and between the ceramic filler particles, their reactivity in combination with the high ceramic yield in air and the low ceramization temperature [11, 15]. The oxide ceramic fillers Al_2O_3 and ZrO_2 have been chosen because they guarantee for the best coating properties in terms of mechanical properties oxidation and corrosion resistance as well as suitable absorption behavior of the laser radiation [27–29]. The resulting ceramic coating systems were characterized regarding their microstructure, friction and wear properties, protection behavior against corrosion and thermal shock resistance.

2. Experimental procedure

2.1. Materials and coating suspension

All materials used in this work are commercially available. The magnesium wrought alloy AZ31B, which is a frequently used in many industrial sectors, with 1 mm in thickness was used as the substrate for the coatings. The magnesium alloy was cut into 40×40 mm sheets, cleaned in acetone by ultrasonic treatment and dried. Two different silazanes, Durazane 2250 (perhydropolysilazane, 20 wt% in di-n-butylether, previously known as PHPS NN120.20) and the liquid (oligo)silazane Durazane 1800, previously known as HTT1800 (both from Merck KGaA, Germany), were used as precursor materials for the bond-coat and as matrix former for the top-coat, respectively. The simplified chemical structures of the silazanes are shown in Fig. 1.

In order to improve the crosslinking-behavior of Durazane 1800, 3 wt% DCP (dicumyl peroxide, Sigma-Aldrich Chemie GmbH, Germany) as an initiator was added to the liquid precursor.

As already mentioned, the high shrinkage of the silazanes of up to 50 vol% during pyrolysis [17], which is caused by mass loss and densification, limits the thickness of ceramic coatings to a few microns [10,11]. Higher coating thicknesses are obtained by the addition of passive and active fillers [15]. Ceramic fillers, in particular Al_2O_3 and ZrO_2 are characterized by their good availability, good mechanical properties (compressive strength and/or flexural strength, hardness), high wear resistance and inertness to a wide range of chemicals.

Therefore, tetragonal ZrO_2 with a mean particle size $d_{50} = 0.3$ µm (3 mol.% Yttria stabilized zirconia, 3YSZ) (ZirPro CY3Z-RS, Saint-Gobain) and α-Al_2O_3 (Alfa Aesar, Germany) with a purity of 99.9 % and a mean particle size of $d_{50} = 0.9$ µm were selected as passive fillers to increase the coating thickness and to improve the surface hardness, wear and corrosion resistance. Both fillers are also characterized by the appropriate thermal resistance for the laser treatment in air.

The two ceramic components form an eutectic system, whereby, depending on the composition, the microstructure, the morphology, the solidification behavior, or the mechanical properties of the coatings are influenced.

For the development of suitable coating compositions, slurries with different filler amounts and precursor fractions were prepared. The volume content of Al_2O_3 in the green coating varied between 18 and 48 vol% and that of ZrO_2 between 8 and 38 vol%. The precursor content was constant at 44 vol% for all coating systems. The preparation of the suspensions started with the dissolution of the dispersant DISPERBYK-2070 (BYK-Chemie GmbH, German) in di-n-butylether (purity > 99 %, Acros Organics BVBA, Belgium). Afterwards, the fillers were added to the solution and dispersed by magnetic stirring and ultrasonic treatment. Finally, the precursor Durazane 1800 was added to the suspension and mixed by magnetic stirring. The solvent content in the suspensions was adjusted according to the filler content as well as to the behavior of the respective fillers in the suspension.

For the selection of the final composition, the number of stress cracks, the resulting microstructure and the morphology of the coatings were investigated after laser treatment. These preliminary tests showed that the best composition was achieved with a hypereutectic composition of the two ceramic fillers, which resulted in a green coating composed of 18 vol% Al_2O_3, 38 vol% ZrO_2 and 44 vol% Durazane 1800. The coatings with this composition were investigated in the further process of this study.

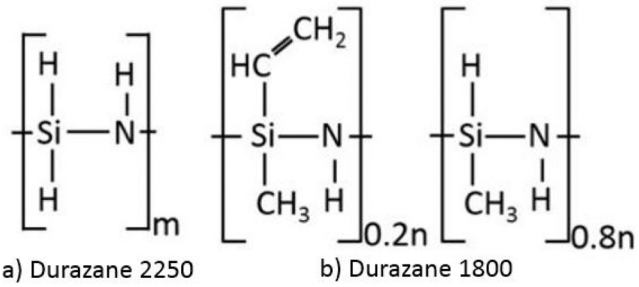

Fig. 1. Simplified chemical structure of the selected silazanes.

2.2. Coating preparation

The cleaned magnesium sheets were dip-coated (RDC 15, Bungard Elektronik GmbH & Co.KG, Germany Switzerland) in the Durazane 2250 solution with a hoisting speed of 0.5 m•min^{-1}. The suitability of the perhydropolysilazane as a bond coat was studied in detail in the work of Günthner et al. [10], Wang et al. [8,12] and Horcher et al. [30]. After drying, the bond-coat was cured in a conventional furnace (N41/H, Nabertherm, Germany) in air only at 150 °C for 1 h to avoid damaging the magnesium substrate leading to the reduction of tensile strength, Young's modulus and hardness, due to crystal recovery and recrystallization [18]. The resulting layer thickness was about 1 μm [10]. The thermal treatment of the bond-coat at 150 °C was sufficient to improve the wetting of the top-coat and to increase the adhesion of the top-coat to the substrate [8,11]. In addition, in air Durazane 2250 forms at temperatures between 150 and 400 °C a dense, crack-free passivating SiO_x layer, which prevents the oxidation of the magnesium substrate during the crosslinking step and the laser treatment [8–10].

The Durazane 1800 based top-coat suspension containing the Al_2O_3/ZrO_2 fillers was deposited on the bond-coat by using a spray coater model 780S-SS (Nordson EFD, USA). The spray parameters were adjusted to obtain a green coating thickness of 40–50 μm. Afterwards, the top-coat was annealed at 150 °C in air for 1 h to dry and to crosslink the coating, which led to better mechanical properties of the green coating for the subsequent laser treatment and an increase in the ceramic yield of the used silazane.

The laser pyrolysis was conducted using a Nd:YVO_4 laser (λ = 1064 nm) (EasyMark 10E, ROFIN-BAASEL Lasertech GmbH Co.KG, Germany) with a focus diameter of about 40 μm at room temperature in air. The laser was operated in a continuous wave mode with a laser power of 10 W and a scanning velocity of 10 mm/s. The best coating properties with regards to the roughness, morphology and mechanical properties were obtained with a distance between two adjacent laser tracks (hatching distance) of 50–55 μm. These parameters allowed complete melting of the fillers and the pyrolysis of the used silazane to obtain dense, ceramic coatings. All experiments were carried out with the coating in focal plane of the laser beam. The adjustment of the laser parameters to generate coatings based on filled organosilazanes are described in detail in preceding studies [26,30].

2.3. Coating characterization

The optical absorption behavior of the crosslinked coating was evaluated by UV–VIS–NIR-spectrophotometry (UV-3600, Shimadzu Corporation, Japan) equipped with an integrating sphere, which enables the determination of the total and diffuse transmittance and reflectance spectra.

The surface and microstructure of the coatings and substrates were examined by a light microscope (Axiotech HAL 100, Carl Zeiss Microscopy GmbH, Germany) and a scanning electron microscope (SEM) (Zeiss Sigma 300 VP, Carl Zeiss AG, Germany). The element composition was determined by using an energy dispersive X-ray spectrometer (EDS) (EDAX Octane Super, EDAX AMETEK GmbH, Germany).

In order to investigate the chemical composition and the degree of conversion of the preceramic polymers after laser pyrolysis, attenuated total reflection infrared (ATR-FTIR) spectroscopy (Tensor 27, Bruker Corporation, USA) was used.

To evaluate the thermal load of the magnesium substrate by the laser radiation, the tensile strength and Young's modulus of the uncoated substrate as well as of the laser treated coated samples were measured and compared by using a tensile testing machine (Zwick Z100/TL3S, ZwickRoell GmbH & Co. KG, Germany) according to DIN EN ISO 6892. This enables the investigation of any mechanical degradation of the substrate material as a result of thermally activated processes.

The adhesion strength of the coatings was evaluated by using a pull-off test (ASTM D4541), with an aluminum dolly with (diameter10 mm), which was glued onto the surface of the coating. After the adhesive was cured, the assembly was attached to an automatic pull-off tester (PosiTest AT-A, DeFelsko Corp., USA). The test device pulls the dolly perpendicular and measures the force necessary to detach it from the surface. The applied pulling rate was 1 MPa•s^{-1}. The test enables the determination of the adhesive strength and the evaluation of the failure mechanism, supported by optical microscopy and SEM. In order to investigate the failure mechanism more precisely, EDS mappings were performed on parts of the tested area.

The microhardness of the coatings was measured by using a hardness tester according DIN EN ISO 14577 (Fischerscope HM2000, Helmut Fischer GmbH, Germany). For this purpose, a symmetrical pyramidal shaped diamond indenter was pressed vertical with a force of 0.098 N into the surface of the sample and the Vickers hardness HV 0.01 (load 98 mN) was calculated from the mean value of the two diagonals of the indenter. In order to avoid the influence of surface roughness on the results, the measurements were conducted on metallographic polished cross-sections.

The wear behavior of the coatings and substrate material towards an abrasive counter body was evaluated by a method, which is based on a linear Taber Abraser test (ASTM D 6279), by using a scratch hardness tester (Lineartester Model 249, Erichsen GmbH & Co. KG, Germany). In this test, the coating is loaded by a counter body, which was covered with a silicon carbide grinding paper, Grit 320 (US #280, particle size 46 μm). The counter body was pressed onto the coated samples with a constant force of 20 N. Subsequently, the samples were moved linearly against the counter body, which was attached to the scratch hardness tester, with a feed speed of 200 mm•s^{-1}. The length of the wear track was 60 mm. The size of the counter body was 25×25 mm. For each sample 500 abrasion cycles were performed, whereby the abrasive paper was replaced after every 100 cycles. After the test, the mass loss per unit area was determined and the worn surface was examined by SEM.

The arithmetic mean roughness value R_a and the averaged roughness depth R_z were measured with a roughness measuring instrument acc. to DIN EN ISO 4287. For the determination of the characteristic values the stylus instrument MarSurf PS10 (Mahr GmbH, Germany) was used.

The sliding friction behavior of the coatings on the magnesium alloy AZ31 was investigated by the pin-on-disc method using hardened and polished steel pins (DIN 1.2367, hardness 580 HV). A surface pressure of 10 MPa and a sliding speed of 10 mm/s have been applied. The tests were conducted at room temperature in linear motions without any coolants or lubricants. The coefficient of friction (COF), which is a dimensionless scalar value and describes the ratio of friction between two bodies, was determined.

The corrosion protection behavior of the laser pyrolyzed coatings was evaluated in a 5 wt% aqueous NaCl solution for 168 h and compared to the corrosion resistance of the pure magnesium alloy. After the corrosion test, the samples were rinsed off with deionized water to remove any corrosion products. Subsequently, the corroded magnesium alloy and the coated samples were examined by SEM and EDS.

Thermal shock tests were carried out on coated magnesium samples to investigate the thermal shock resistance of the ceramic coating system. For this purpose, the samples were first immersed in liquid nitrogen (-196 °C) for 15 min and then immediately placed in an oven heated to 400 °C (Nabertherm LH 60/14, Nabertherm GmbH, Germany) for 15 min. This cycle was repeated five times and subsequently the effects of the thermal shock tests on the samples were evaluated by SEM investigations.

3. Results and discussion

3.1. Laser pyrolysis of the coating

3.1.1. Absorption behavior

The most important requirement for laser treatment of the coatings is that the laser radiation is almost completely absorbed within the

coating. The resulting generation of very high temperatures led to the ceramization of the silazane and the melting of the ceramic fillers, which enabled the formation of a dense coating. In addition, it prevented the interaction between the substrate and the laser radiation and any laser-induced damages of the substrate like degradation of the mechanical properties because of changes in the microstructure or even melting of the magnesium alloy. It is decisive, that the absorption occurs uniformly in the whole volume of the coating in order to ensure the pyrolysis and ceramization of the coating over the entire thickness.

For these reasons, the coating must be opaque to the laser radiation, which means that the transmission over the entire coating thickness should be zero at the wavelength of the laser radiation. However, the amount of laser energy lost through reflection at the surface of the coating may be kept low in order to ensure that a sufficient amount of laser power is absorbed.

To evaluate the absorption and transmission behavior of the green coatings, the transmission and the total reflection were measured by UV–VIS–NIR spectrophotometry (Fig. 2).

The reflection behavior was measured in a wavelength range between 200 and 1500 nm. The total reflection in this range was 10 – 80 %. The peak at 880 nm is a noise signal associated with the change of the detector during the measurement. At 1064 nm, the wavelength of the used Nd:YVO_4 laser, the reflection was about 57 % (Fig. 2a)). Fig. 2b) presents the transmission spectrum of the green coating on a 1 mm fused silica substrate in a wavelength range of 200–1500 nm. The fused silica substrate was selected for the transmission measurements because of its higher transmission in the spectral range from UV to IR compared to other optical glasses, minimizing interferences. As can be seen in Fig. 2b), the transmission through the 40 μm thick green coating was almost zero over the entire wavelength range. Consequently, thermal loading by heating or melting of the substrate due to an interaction between the laser radiation and the magnesium substrate can be excluded. Considering that the total reflection was 57 %, it can be concluded that the absorption was approximately 43 %, which means that a high proportion of the laser energy was available for the pyrolysis of the precursor and melting of the fillers. The measured values confirmed that the coating composition was suitable for the ceramization of this coating type with the chosen Nd:YVO_4 laser. According to these results, the laser parameters described in Section 2.2 were determined for the complete ceramization of the coatings without thermally stressing the substrate. The high absorption capability of the coating system was mainly caused by the high filler content and the small particle size of the fillers ($d_{50} < 1$ μm), which were in the same size range as the wavelength of the Nd:YVO_4 laser used, which led to an increase in scattering effects of the radiation within the coating. This in turn resulted in the increase of the optical path length and in an increase of the extinction coefficient leading to a homogeneous laser absorption in the entire coating volume [23,31].

3.1.2. Surface morphology

The absorption of the laser radiation and the resulting pyrolysis of the coating effect its surface structure and roughness (Fig. 3).

The surface of the green coating (Fig. 3a)) was homogenous, smooth, free of surface defects and open porosity. The arithmetic mean height R_a was 0.3 ± 0.1 μm. In contrast, after the laser pyrolysis (Fig. 3b)) the surface was structured and the R_a value of the coating increased to 2.6 ± 0.2 μm. The surface structuring resulted predominantly from the melting of the ceramic fillers during the laser treatment. The resulting melt pool dynamics as a consequence of the Marangoni convection, determines the surface morphology [32]. The convection flow in the melt pool is attributed to the temperature gradient at the surface of the melt pool. Due to the Gaussian intensity distribution of the laser radiation with a maximum in the beam center, a temperature gradient in radial direction arose. Therefore, in the center of the melt pool the temperature was higher than in the peripheral areas. The temperature gradient results in a surface tension gradient, since the surface tension σ depends on the temperature T. The surface tension gradient in radial direction r is described by Eq. 1 [33,34].

$$\frac{\partial \sigma}{\partial r} = \frac{\partial \sigma}{\partial T} * \frac{\partial T}{\partial r} \tag{1}$$

For $\partial\sigma/\partial r < 0$ the temperature field at the surface results in a stress distribution with small values in the middle and larger values at the edge of the melt pool. The gradient caused by a near-surface melt pool flow from the center to the edge, resulting in the characteristic structuring with an accumulation of material at the edge area [34]. The structures had a width of about 50 μm, which in turn corresponded approximately to the focus diameter. The increase of the surface roughness was a result of this structuring phenomena. The laser treatment led also to a color change of the coating and turned from white to dark gray/black, indicating the presence of "free" carbon. Trassl et al. [35] described the formation of so-called “free” carbon within an amorphous SiCN phase during pyrolysis of organosilazanes in a conventional furnace in inert gas atmosphere. However, Müller et al. [36] also confirmed the generation of free carbon during laser pyrolysis of an oligomethylvinylsilazane. But, also oxygen vacancies formed in the Al_2O_3- and ZrO_2 phases can contribute to the color change [37]. It is known, that laser irradiation on ZrO_2 may induce the formation of oxygen vacancies within the crystal lattice, which act as absorption centers, increasing the overall absorption of the laser radiation and thus enabling the laser pyrolysis

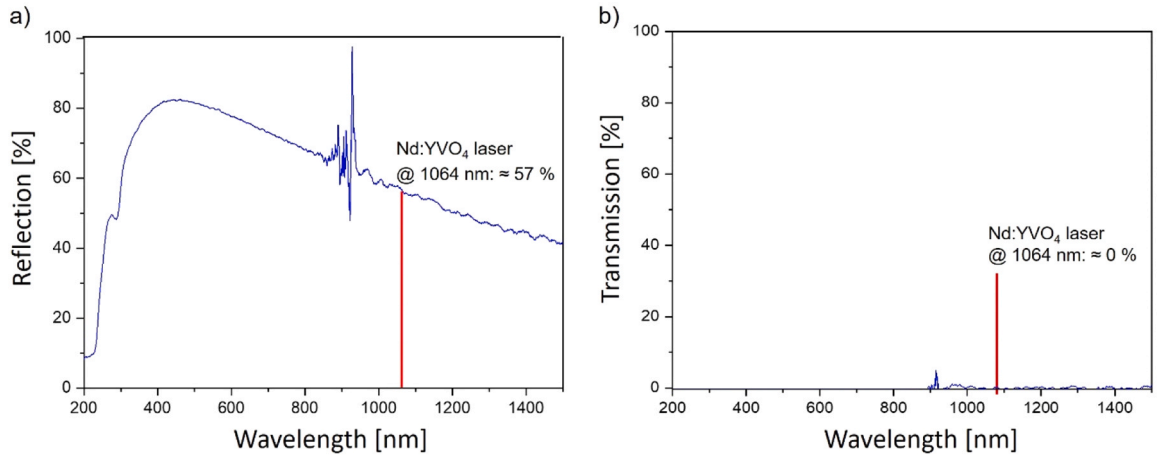

Fig. 2. UV–VIS–NIR measurements of a 40 μm thick green Al_2O_3/ZrO_2 organosilazane based composite coating on a 1 mm thick fused silica substrate: a) total reflection; b) total transmission; the red line represents the wavelength of the used Nd:YVO_4 laser.

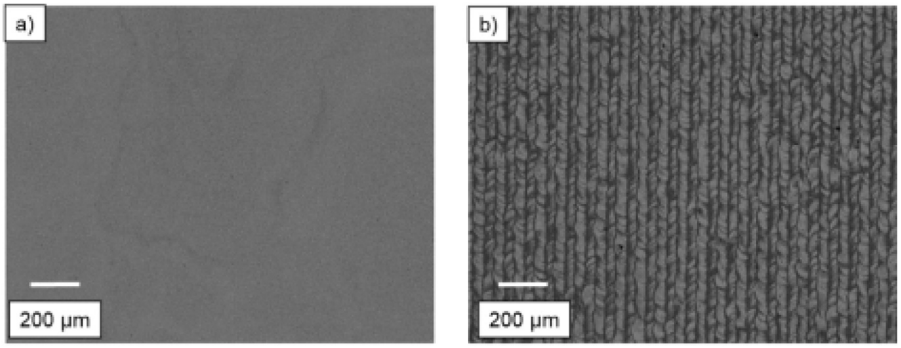

Fig. 3. SEM micrographs (backscattered electrons, BSE) of the coating surface a) green-coating b) laser pyrolyzed coating.

[38].

3.1.3. Microstructure

The SEM micrograph of the cross-section (Fig. 4a)) of the green Al_2O_3/ZrO_2-filled silazane-based composite coating illustrates, that the Al_2O_3 particles (dark regions) were distributed homogeneously, embedded in a ZrO_2-rich (bright regions) silazane matrix (Fig. 4a). The precursor acted as a binder between the individual filler particles, resulting in pore- and crack-free green coatings. The homogeneous distribution of the fillers is a precondition for the uniform absorption of the laser radiation over the entire coating volume. The SEM micrograph also indicated a good wetting of the composite coating on the bond-coat after spraying, because no defects were detected at the interface. This point is a very important prerequisite for the formation of well adhering coatings during laser pyrolysis.

After the laser treatment the individual and separated particles disappeared (Fig. 4b). Remarkably, no pores and no cracks at the interface to the substrate were observed, which indicates an excellent adhesion of the coating system. The micrographs demonstrated the compaction of the green coating as a result of the laser pyrolysis. Thus, ceramic coatings with a thickness of 15–20 µm were generated from green coatings with an initial thickness of 40 µm, which means a shrinkage of about 60 %, due to the shrinkage of the precursor amount during ceramization and the complete melting of the fillers leading to the elimination of microporosity. However, it cannot be excluded that the coating material was partially evaporated during laser treatment [23,30].

Fig. 4b and 5 show the formation of a predominant dendritic microstructure of the coating after the laser treatment, which is a result of a complete melting of all components with the subsequent rapid solidification of the melt. Nevertheless, a planar or fine-grained structure has formed in the vicinity of the magnesium substrate due to the high thermal conductivity of the magnesium alloy, which led to high temperature gradients and cooling rates at the interface between the coating and the substrate [34,39]. With increasing distance from the substrate, the heat was increasingly dissipated into the already solidified coating areas, which have a lower thermal conductivity than the magnesium substrate. This led to a reduction of the temperature gradient, resulting in a transition to a cellular/columnar-dendritic solidification structure [34,39,40]. Fig. 5a) gives an overview about the solidification microstructure over the cross-section. The fine-grained structure and the cellular/columnar-dendritic structures in a higher magnification as well as the transition region, marked by red dashed line, are displayed in Fig. 5b).

The effect of the temperature gradient on the grain morphology is shown in Fig. 6 in a schematic visualization of grain structure evolution.

Fig. 7 shows the element mappings of the laser pyrolyzed coating investigated by energy dispersive X-ray spectroscopy (EDS). In the examined area the main chemical elements of the coating silicon (Si), zirconium (Zr), oxygen (O) and aluminum (Al) were detected. The main element of the substrate was magnesium.

The surface of the coating exhibited an enrichment of the elements oxygen, silicon and to some extent of aluminum. The enrichment of silicon on the surface of the coating results from the partial evaporation of the polysilazane during laser treatment and subsequent recondensation. The interaction between the laser and the coating occurs within a few milliseconds, reaching extremely high temperatures above the melting point of ZrO_2 (> 2710 °C [41]). This fast and excessive heating led to a partial laser-induced vaporization of the polysilazane, resulting in a splitting off of gaseous Si containing compounds [23]. Since the heating with the laser affects only a very small area, a steep temperature gradient to surrounding areas arises. Therefore, the vaporized components recondense in the immediate vicinity and form a fine particulate precipitation on the surface. However, this precipitation could easily be removed with a cloth, as the adhesion to the underlying coating was very weak. This observation is in a good agreement with previous results [25,26,30].

Apart from the surface, the microstructure of the coating was composed of ZrO_2 primary crystallites and an Al_2O_3 containing phase

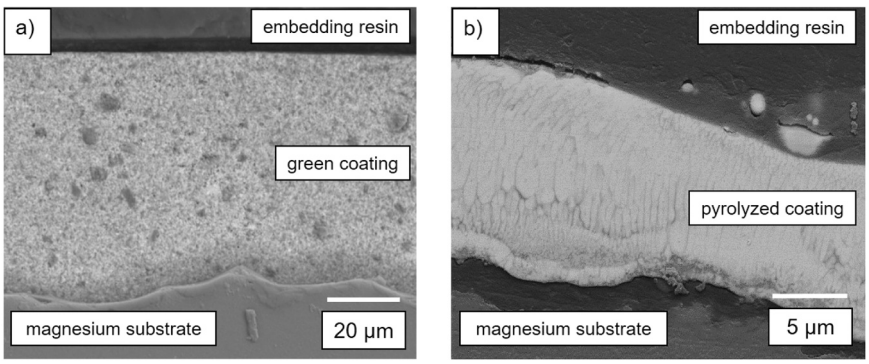

Fig. 4. Cross-section SEM micrographs of the Al_2O_3/ZrO_2-filled oligosilazane-based coating a) before laser pyrolysis, b) after pyrolysis.

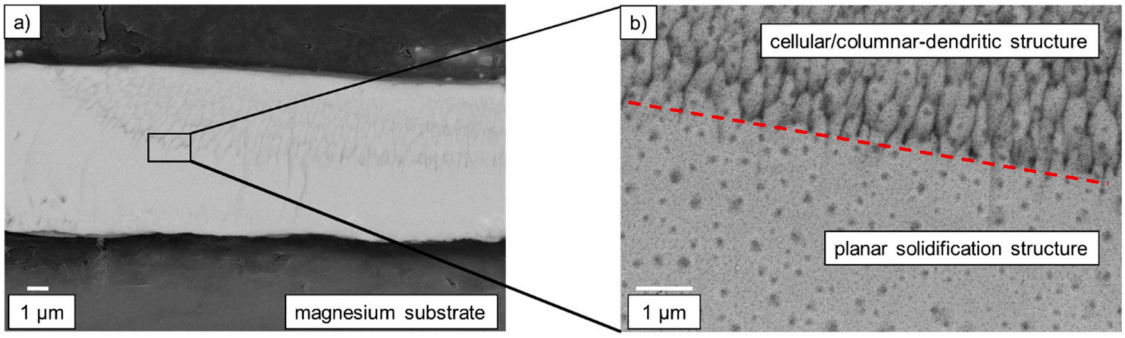

Fig. 5. Cross-section SEM micrographs of the laser pyrolyzed Al_2O_3/ZrO_2-filled oligosilazane-based composite coatings a) overview, b) transition between planar and cellular/columnar dendritic solidification.

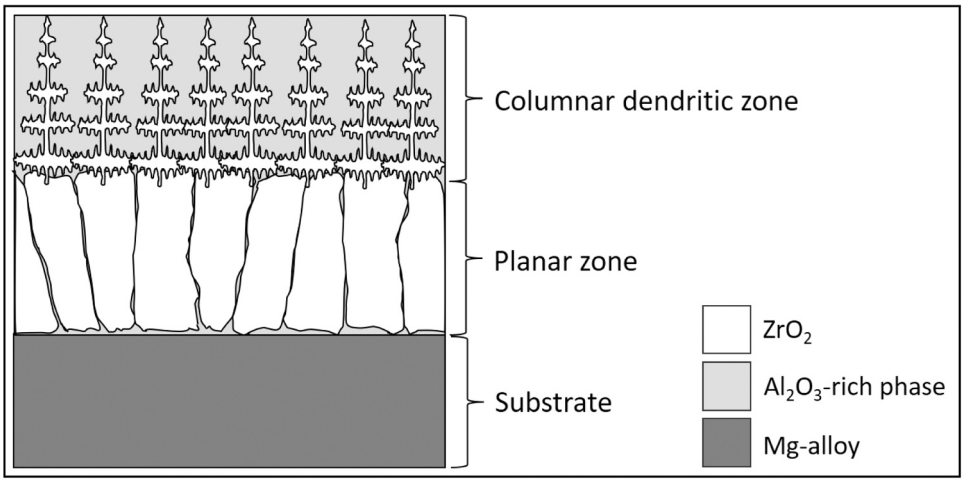

Fig. 6. Schematic visualization of grain structure evolution during laser pyrolysis.

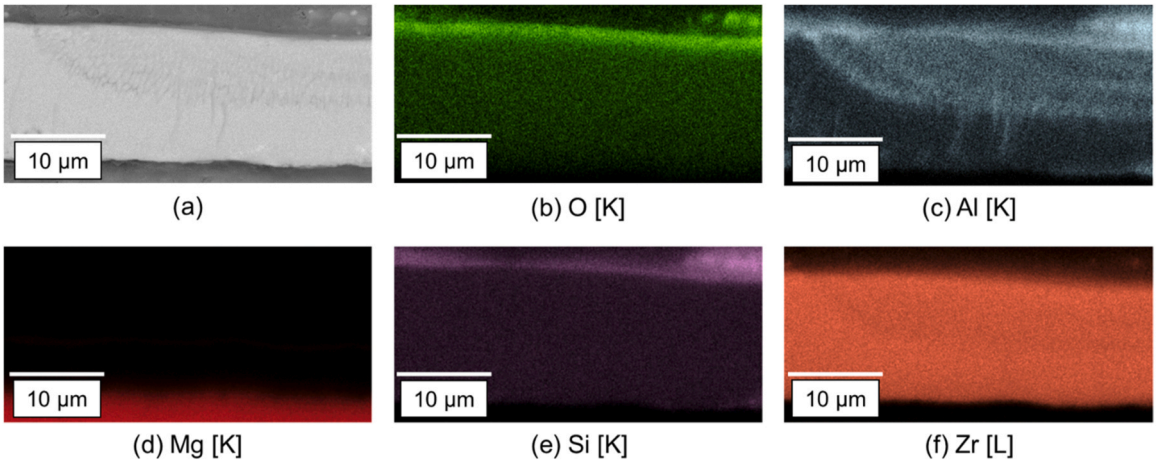

Fig. 7. a) SEM-image with EDS-mappings of the elements b) oxygen (O), c) aluminum (Al), d) magnesium (Mg), e) silicon (Si), f) zirconium (Zr) of the coating after laser pyrolysis.

preferentially enriched between the ZrO_2 dendrites. Due to the hypereutectic composition, at first ZrO_2 primary crystallites were formed. When reaching the solidus temperature, the residual Al_2O_3-rich melt solidifies. A low enrichment of silicon between the dendrites has also been detected in the EDS investigations, which is evidence that the precursor only partially evaporated during laser treatment. The interface to the substrate was well defined and neither diffusion of elements from the coating into the substrate nor the diffusion of magnesium into the coating were detected, because during laser pyrolysis the interaction time was too short for a diffusion-controlled processes. In addition, the high thermal conductivity of magnesium led to a fast removal of the generated heat.

3.1.4. FT-IR spectroscopy of the coating system

The polymer-to-ceramic conversion of the silazane within the coating was investigated by FTIR-spectroscopy before and after laser

pyrolysis (Fig. 8).

The FTIR-spectrum of the green coating showed the characteristic bands of the structure of the used silazane. Methyl groups (Si-CH_3) at 1260–1275 cm^{-1}, C(sp^3)-H at 2963 cm^{-1}, N-H at 3400 cm^{-1} and Si-H at 2160 cm^{-1}. In the fingerprint region, the absorption bands between 1000 and 800 cm^{-1} indicate the presence of Si-C-Si and Si-N-Si bonds. In addition, two bands between 1200 and 1000 cm^{-1} and at 790 cm^{-1} were detected, which are characteristic for Si-O-Si bonds resulting from crosslinking reactions between the Si-H and Si-N bonds of the precursor and oxygen from air or moisture, forming reactive silanol groups, which in turn formed Si-O-Si bridges via condensation reactions [42–44], which led to a sufficient crosslinking of the organosilazane based green coatings for the subsequent laser treatment.

After laser treatment of the coating no organic groups or hydrogen-containing functional groups of the silazane (N-H and Si-H) were detected, which indicates fully ceramization of the precursor. However, the bands of the Si-O-Si groups were still identified between 1200 and 1000 cm^{-1}, whereas the Si-N and Si-C bonds of the silazane were no longer detected by FT-IR spectroscopy. On the one hand, it is conceivable that the weak signals may be superimposed by the signals from the Si-O bonds. On the other hand, it must be considered that the rapid energy absorption by the precursor during laser pyrolysis led to immediate bond cleavage and vaporization, followed by an oxidation reaction forming chemical compounds like SiO_x [19,23]. The absorption bands detected at 760 and 580 cm^{-1} can be assigned to the ZrO_2 and at 513 cm^{-1} to the Al_2O_3 filler.

Due to the short interaction time during laser treatment, no additional crystalline products detectable with XRD were formed. Only signals from the fillers as used in the green coating appeared. Therefore, the XRD results are not explicitly described

3.1.5. *Influence of the laser pyrolysis on the substrate material*

An important prerequisite for the successful laser-based processing of ceramic coatings via the precursor route on low-melting metals like magnesium is to guarantee, that the laser energy does not impair the mechanical properties of the substrate. Melting of the magnesium substrate by the laser treatment of the coating could be excluded by the examination of the cross-section micrographs (see Figs. 4 and 5) but this investigation gives no information about a reduction in the mechanical properties because of thermally induced processes like crystal recovery and subsequent recrystallization [45]. Therefore, the influence of the laser treatment on the Young's modulus and tensile strength of the uncoated and coated magnesium substrate were investigated (Fig. 9). For

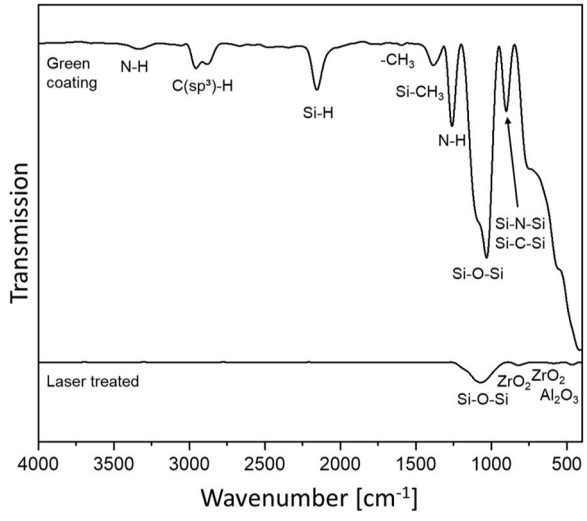

Fig. 8. FTIR spectra of a green coating and the laser treated Al_2O_3/ZrO_2-filled organosilazane based coating.

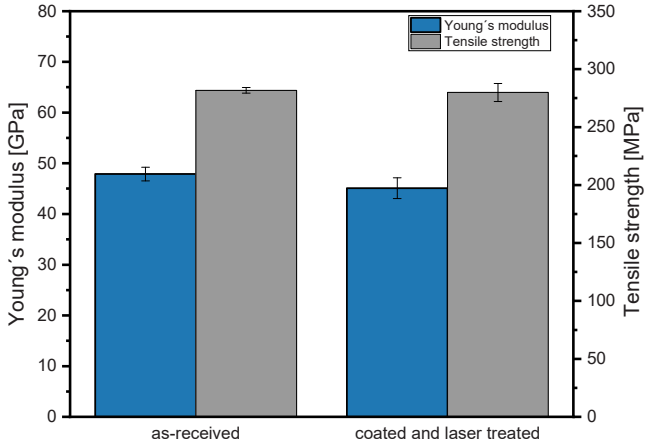

Fig. 9. Young's modulus and tensile strength of the magnesium substrate as-received and after laser pyrolysis of the coating.

the measurements the coating was not removed from the magnesium substrate, because of its small thickness in comparison to the substrate. Beside this, the limited ductility of the ceramic coating in comparison to magnesium during the tensile test led to its detaching from the substrate. Therefore, an influence of the coating on the tensile strength and Young's modulus can be excluded [30].

As can be seen from Fig. 9, the ceramization of the coating via laser treatment has no influence on the mechanical properties of the magnesium substrate, which excludes a thermal load. This result confirms the absorption measurements of the coating system described above, that the laser energy was completely and uniformly absorbed within the coating volume leading to the melting of the ceramic fillers and the ceramization of the organosilazane. Beside this, the interaction time between the laser beam and the coating is only in a range of milliseconds because of the scanning process and the beam diameter related to the substrate volume was very small, which avoided heat accumulation of the substrate. Moreover, the residual heat was dissipated due to the high thermal conductivity of the magnesium substrate.

3.2. *Coating properties*

3.2.1. *Adhesive strength*

To demonstrate the potential of laser pyrolyzed ceramic coatings on magnesium substrates, the mechanical properties as well as the capability to protect the substrate from corrosive media and against abrasive wear were investigated. Magnesium alloys have a comparatively low hardness and poor abrasive wear resistance, which should be significantly improved by the generated ceramic coating. A prerequisite to meet these expectations, is an excellent adhesion to the substrate without defects like cracks and pores.

To quantify the adhesive strength, pull-off adhesion tests (ASTM D4541) were performed. The determined average pull-off adhesive strength of the laser pyrolyzed coating on the magnesium alloy was 25.9 ± 2.7 MPa. There are two main reasons for the excellent adhesion. Firstly, the laser pyrolyzed coating itself as well as the interface to the substrate were dense and free of pores as shown in Figs. 4 and 5. It is known that a defect above a critical size can induce a macroscopic failure under tensile load, which leads to a reduction in adhesive strength [46]. Secondly, the silazane formed chemical bonds with both the metallic substrate and the fillers, which improved the adhesion of the coating to the substrate and the cohesion within the coating [10,47]. Moreover, the rough surface of the magnesium substrate increased the adhesion of the coating system by mechanical interlocking and increased the number of covalent bonds by increasing the effective surface. A high adhesion strength is an important prerequisite for wear protective coatings, because this allows the transfer of loads from the

coating to the substrate without coating failing or flaking off.

To assess the failure mechanism, light microscope images of the coating after pull-off tests were evaluated (Fig. 10). To determine whether adhesion failure occurred between the substrate and the bond-coat or between the bond-coat and top-coat, EDS measurements were performed in a representative part of the tested area, which is indicated by the red rectangle in Fig. 10.

The EDS-mappings of magnesium and oxygen showed by their predominant occurrence that the coating system failed mainly at the interface between the bond-coat and the substrate. However, silicon was only detected in a few areas, resulting from Durazane 2250 which filled grooves and rolling marks of the magnesium sheet during the application of the bond-coat by the dip-coating process. In these areas, adhesion failure occurred between the top-coat and the bond-coat, because the adhesion between the substrate and bond-coat was enhanced by mechanical interlocking. The mapping of zirconium identifies the areas where the top-coat became exposed, indicating a cohesion failure within the top-coat but in only few areas. Therefore, the adhesion between the substrate and the bond-coat was the limiting factor, which can be attributed to the uneven distribution of the bond-coat because of the rough surface of the magnesium substrate. In addition, due to the low crosslinking temperature of the bond-coat (150 °C), the adhesion to the substrate was lower than the bonding within the top-coat itself, which is completely chemically bonded due to the melting and solidification of the fillers by the laser treatment.

Due to the large number of different kinds of surface treatments and coating systems developed for the protection of magnesium materials, a direct comparison of the adhesive strength depending on the coating method is rather difficult. However, for a ceramic Al_2O_3-based coating on magnesium applied by ion beam sputter deposition and ion beam assisted deposition adhesive strengths of 18 and 34 MPa were reported [48]. However, the application of such coatings requires vacuum processes, leading to high costs. Anodic oxidation is another option to obtain ceramic surfaces on magnesium alloys. A commercial process for producing a ceramic-like surface is the so-called Magoxid-Coat® process, in which the surface of the magnesium alloy is ceramized by a plasma chemical reaction in an electrolyte, whereby the adhesive strength to the substrate is specified as at least 30 MPa [4]. However, anodically oxidized coatings are porous, so additional steps are necessary for optimal corrosion protection. Thus, the laser pyrolyzed PDC-based protective coating had a comparable adhesion strength with other coating systems, whereby the laser pyrolysis leads to predominantly dense coatings, produced without vacuum processes.

3.2.2. Hardness

The hardness measurements were conducted on metallographic polished cross-sections to exclude the influence of surface roughness. The applied load during these measurements was 98 mN, which corresponds to the Vickers Hardness HV 0.01.

The average determined hardness of the laser pyrolyzed coating was 19.79 ± 1.90 GPa (HV 0.01) in comparison to magnesium alloy AZ31B with only 0.67 ± 0.01 GPa (HV 0.01). This demonstrates the striking increase in hardness of the surface.

Table 1 displays an overview of the hardness values of the coatings

Table 1
Selected coating methods and coating systems on magnesium alloys and the corresponding coating hardness in GPa. For comparability, the Vickers hardness values were converted in SI units [GPa].

Process	Coating components or composition	Alloy	Vickers hardness [GPa]	reference
PVD	AlN/TiN	MgAl9Zn1	1.0 (HV0.5)	[50]
PVD	CrN	MgAl3Zn1	≈ 12.5 (n.s.)	[51]
PVD	TiN	MgAl3Zn1	≈ 16.2 (n.s.)	[51]
PVD	(TiAl)N	MgAl3Zn1	≈ 17.8 (n.s.)	[51]
PVD	TiN/AlN	MgAl3Zn1	≈ 13.8 (n.s.)	[51]
PVD	NbN/CrN	MgAl3Zn1	≈ 14.0 (n.s.)	[51]
CVD	Ti/DLC/DLC	MgAl9Zn1	19.45 (HV 0.001)	[52,53]
PVD	Ti/Ti(C,N)/CrN	MgAl9Zn1	21.55 (HV 0.001)	[52,53]
PVD	Cr/CrN/CrN	MgAl9Zn1	19.38 (HV 0.001)	[52,53]
PVD	Cr/CrN/TiN	MgAl9Zn1	18.78 (HV 0.001)	[52,53]
PVD	Ti/(Ti,Si)N/(Ti,Si)N	MgAl9Zn1	16.88 (HV 0.001)	[52,53]
Laser cladding	Al_2O_3	MgAl9Zn1	≤ 19.23 (n.s.)	[54]
Laserpyrolysis	silazane, Al_2O_3, ZrO_2	AZ31B	19.79 (HV 0.01)	this work

n.s.: not specified.

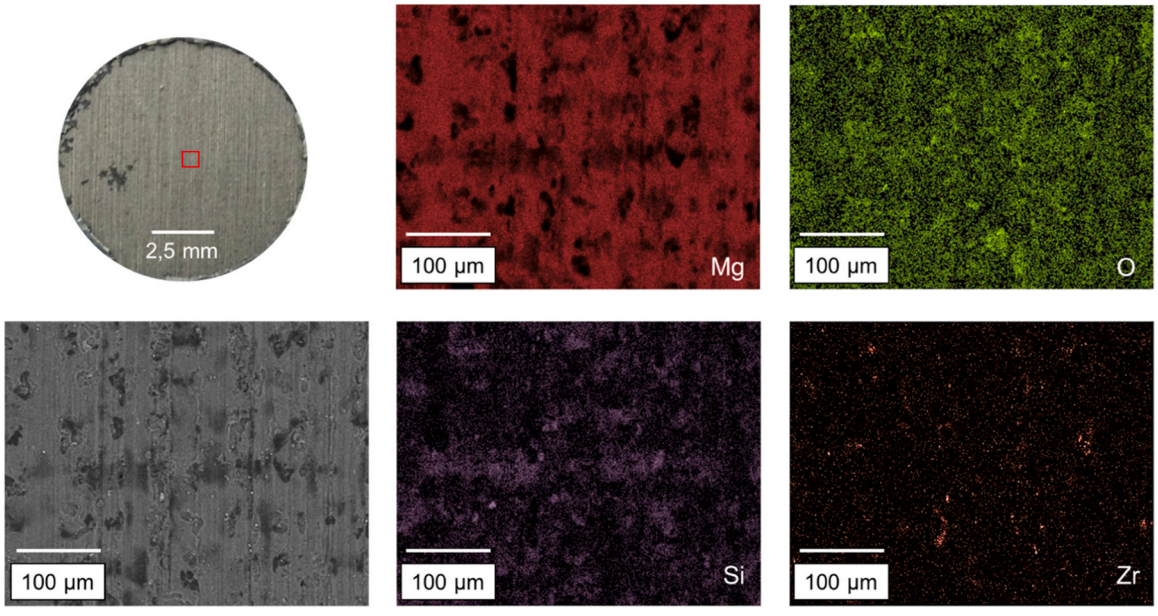

Fig. 10. Light microscope image and EDS mapping of the examined area after a pull-off test of the laser pyrolyzed Al_2O_3/ZrO_2-filled organosilazane based coating. The red rectangle marks the region investigated by EDS.

on different magnesium alloys applied by various methods. Here, only coatings are cited, which were tested with a comparable load, since the hardness values in this test strongly depends on the applied test force [49]. Comparing the values in Table 1 it is obvious that the hardness of the laser pyrolyzed coating system (19.79 ± 1.90 GPa) is comparable or even higher than those for other coatings on magnesium. Considering the substrate impairment and the complexity of the other methods listed in Table 1 the processing of ceramic coating via laser treatment offers great advantages. For example, during laser cladding the magnesium substrate melts in the heat-affected zone, which might influence the mechanical properties of the substrate, whereas during laser pyrolysis a thermal load could be excluded. In addition, the equipment requirements are significantly lower compared to low pressure and vacuum processes such as chemical vapor deposition (CVD) and physical vapor deposition (PVD).

The high hardness values of the laser-treated Al_2O_3/ZrO_2-filled organosilazane coating is attributed to the microstructure and the composition. By combining both ceramic fillers, a synergistic effect can be achieved, which leads to an improvement of the property spectrum. Compared to pure ZrO_2, the addition of Al_2O_3 improves the mechanical properties of the coating system with a simultaneous reduction in density. In addition, an increase in hardness and Young's modulus and an increase in flexural strength are obtained [55,56]. Furthermore, the eutectic system reduces the solidification temperature compared to the pure materials, thus reducing the temperature gradient between the molten regions and the surrounding areas during laser treatment. This is associated with a reduction in thermally induced stresses and consequently with a minimization of stress cracking [55].

As shown in Figs. 4 and 5, the melting of the hard ceramic fillers and the pyrolysis of the organosilazane led to a pore-free ceramic coating. The non-porous microstructure avoided collapse of the coating or crack initiation by compressive load, which increased the mechanical resistance of the coating against penetration of the counterpart [57,58].

In addition, the solidification structure had a significant influence on the hardness. As shown in Fig. 5, a planar and fine dendritic microstructure was formed during laser pyrolysis, which contributed to the increase in hardness, since it counteracted plastic deformation more effectively and reduced the size of the plastic zone [49]. The hardness of ceramic materials also depends on the grain size d and obeys for ZrO_2- and Al_2O_3-based materials with grain sizes above 1 μm the Hall-Petch relationship ($H \approx 1/\sqrt{d}$) [41,59]. That means, the fine-grained microstructure of the laser-treated coatings also contributed to the high resulting coating hardness.

3.2.3. Friction and wear behavior

In designing components made from magnesium, the low hardness and the resulting low wear resistance must be considered. Ceramic coatings are particularly suitable for increasing the abrasion resistance of metallic substrates, due to the high hardness, corrosion and temperature resistance and because of their low density advantageous for lightweight components [60]. However, the wear resistance of a coating also depends on other factors such as coating morphology, fracture toughness, adhesion of the coating to the substrate and surface roughness [46,60,61]. In addition, the coefficient of friction (COF) plays a crucial role and should be kept as low as possible to avoid sliding wear.

To evaluate the wear resistance of the coating as well as of the uncoated magnesium substrate, abrasion tests were carried out with a testing device, which was based on the linear Taber Abraser test. The evaluation was performed by determining the area-related mass loss, surface roughness and by means of SEM investigations. The coefficient of friction (COF) for sliding friction (dry) was determined by pin-on-disc tests using a polished steel pin on both coated and uncoated substrates.

A low coefficient of friction of 0.06 ± 0.01 was determined on the cleaned magnesium substrate resulting from the presence of a thin surface layer, which consisted of $Mg(OH)_2$ and MgO [3,7], acting as a lubricant during sliding of the pin over the substrate surface [62–64]. On the laser pyrolyzed coating, the COF was 0.21 ± 0.02. The higher COF compared to the uncoated magnesium substrate can be attributed to the absence of a lubricating film at the surface and the high surface roughness (R_a = 2.6 ± 0.2 μm) in combination with the high hardness. Since the steel pin had a lower hardness (5.69 GPa) than the pyrolyzed coating (19.79 ± 1.90 GPa), penetration of the steel pin into the layer and thus a mechanical interlocking (form-fit) could be excluded. Therefore, the tribological behavior between the polished steel pin and the coating was significantly influenced by the surface roughness [65]. In sliding friction on hard coatings, surface irregularities have an abrasive effect on the counter body, which in turn increases the frictional resistance and leads to an increase of the COF [66].

In a previous study [25] a COF of 0.33 for a laser pyrolyzed glass/-ZrO_2-filled organosilazane based composite coating was determined. Cross et al. [67] investigated the coefficient of friction between furnace pyrolyzed polycarbosilazane-based bulk samples and a Si_3N_4 counterpart, whereby a COF between 0.2 and 0.7 was reported depending on the surface pressure. Klaffke [68] investigated the friction behavior between steel and various ceramics (Al_2O_3, SiC, Si_3N_4 and ZrO_2) at room temperature for unlubricated reciprocating sliding motion. The COF values published for the respective ceramics were: 0.4–0.5 for Al_2O_3, 0.3–0.5 for SiC, 0.5–0.6 for Si_3N_4 and 0.3–0.5 for ZrO_2 [68]. Compared to the data from the literature, the coefficient of friction of the laser pyrolyzed coating investigated in this work was even lower. However, it must be emphasized that the COF is a system parameter and depends on many measuring and material conditions such as the couple of materials, surface quality, applied load, temperature, and humidity. Therefore, a complete comparability cannot be guaranteed.

While the COF describes the friction behavior and depends strongly on the surface quality, additional properties such as hardness and adhesion between the coating and the substrate are important for the wear resistance of coatings [60], which were investigated in this study with a testing device, based on the linear Taber Abraser test.

Fig. 11 shows SEM images of the surface of the uncoated magnesium substrate and of the laser pyrolyzed Al_2O_3/ZrO_2-filled organosilazane based composite coating after 500 abrasion test cycles with the SiC-abrasive paper covered counter body.

On the surface of the magnesium alloy, scratches and traces were visible. Due to the relative movement and the applied load of the counter-body, the SiC-particles penetrated the magnesium substrate and removed material from the surface of the much softer magnesium alloy. The surface of the coating, on the other hand, did not have any pronounced wear pattern. No material chipping, cracks, or grooves were observed.

In order to quantify the wear behavior of the coating and the substrate material, respectively, the area-related mass loss was determined after 500 cycles. The high abrasive wear on the surface of the magnesium substrate was 34.31 ± 4.89 g/m^2. Due to the relative motion and the applied load of the counter-body, the SiC particles penetrated the metal substrate and removed material from the surface [69]. In addition to the material loss, the abrasive wear also led to an increase in the surface roughness. In Table 2 the arithmetic mean roughness value R_a and the averaged roughness depth R_z before and after the abrasion tests are listed. After the abrasion test, the roughness parameters of the uncoated magnesium alloy increased more than twofold, which is related to the material removal and the insertion of grooves and furrows.

Although there were no visible signs of abrasion on the SEM images of the laser pyrolyzed coating after 500 cycles (Fig. 11), an area-related mass loss of 5.64 ± 0.24 g/m^2 was determined, which was significantly lower than that of the uncoated magnesium substrate. The mass loss of the coating resulted from the initial roughness of the coating. At the beginning of the abrasion test, the SiC-particles of the counter body were only in contact with the roughness peaks of the coating, which means that the real contact surface was significantly smaller than the projected area of the counter body [63].

Therefore, the total applied force acted only on these roughness

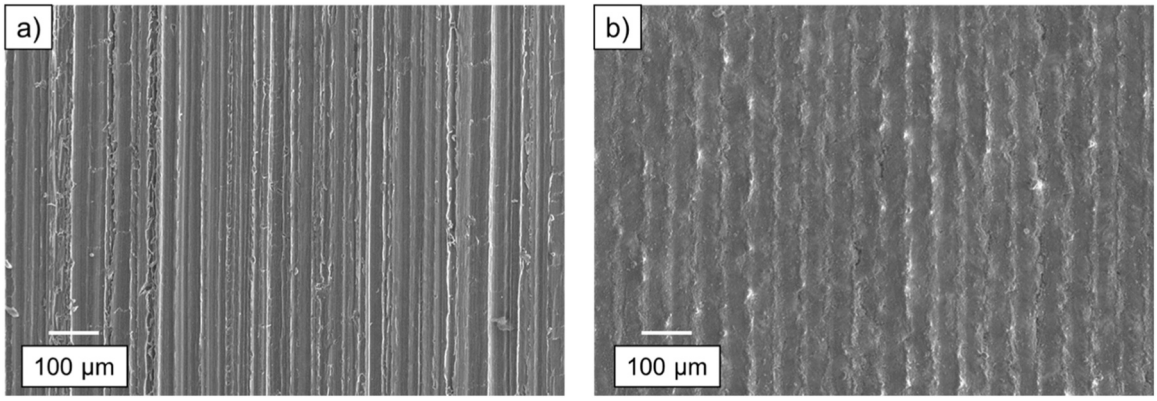

Fig. 11. SEM images of the surface of the uncoated magnesium alloy and of the laser pyrolyzed coating after 500 cycles with the linear Taber Abraser tester, a) uncoated magnesium alloy, b) laser pyrolyzed coating.

Table 2
Surface roughness of the magnesium substrate and of the coating before the abrasion test and after 500 cycles.

Sample		R_a [µm]	R_z [µm]
Uncoated magnesium substrate	as received	2.09 ± 0.15	15.86 ± 1.09
	after 500 cycles	4.53 ± 0.28	31.43 ± 1.61
Laser pyrolyzed coating	as received	2.53 ± 0.18	18.60 ± 2.37
	after 500 cycles	2.23 ± 0.21	15.16 ± 1.62

peaks, leading to high punctual pressure loads. These regions are responsible for the initial friction and interaction between the two bodies and contributed mainly to material loss [63]. With increasing load or duration, the asperities were plastically deformed and removed by the applied shear stresses, whereby the surface was levelled and consequently the applied normal force was distributed over a larger area [63]. The roughness values in Table 2 illustrate the decreasing roughness and the levelling of the surface, due to the removed roughness peaks. Because of their hardness, the removed and loose ceramic particles also accumulated between the coating and the counter-body, rounding off and thus did not contribute further to wear [70]. The mobility of the rounded wear particles and their adaptation to the relative speed, led also to the reduction of wear with increasing test duration and to a decrease in the wear rate after the initial surface leveling [71,72]. This behavior is illustrated by Fig. 12, which shows the area-related mass loss cumulatively after each 100 cycles.

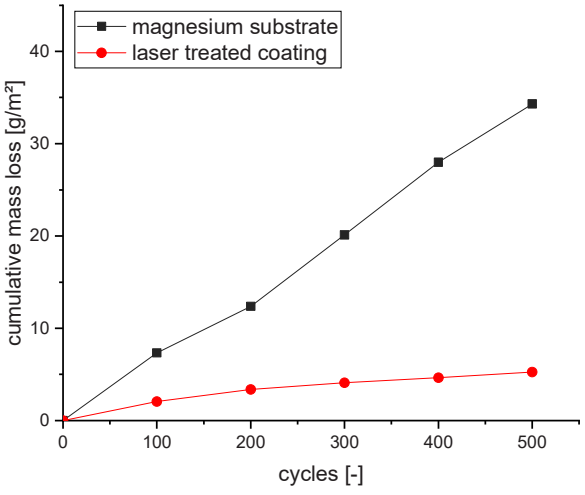

Fig. 12. Cumulative mass loss after each 100 cycles by the linear Taber Abraser test with SiC paper.

For the uncoated substrates, the material loss behaved almost linear. For the ceramic coating, the material loss was also linear up to 200 cycles, although the slope was significantly lower compared to the magnesium substrate because of the higher hardness. The curves flattened off with an increasing number of cycles due to the described material removal occurred predominantly during the first 200 cycles, where mainly the roughness peaks were removed. Subsequently, the applied normal force was distributed over a larger area and the surface pressure was reduced. The decrease in surface roughness and surface pressure led to a reduction in the wear rate.

Even after 500 test cycles, no spalling or delamination of the ceramic coating was detected, which was attributed to the very good adhesion of the coating. The adhesion of the coating on the substrate is of crucial importance, since stresses are transmitted to the ductile substrate, which adapts elastically to the load and thus shear during surface contact did not result in delamination [46]. In summary, the laser pyrolyzed coatings are characterized by a high wear resistance, which effectively protected the substrates from abrasive wear, which also allows use under higher tribological loads.

3.2.4. *Corrosion protection behavior*

Another disadvantage of magnesium is the poor corrosion resistance, which limits its use in corrosive environments, especially with increasing humidity [73]. Likewise, gases such as CO_2 and SO_2 have a negative influence on atmospheric corrosion [73]. Magnesium alloys are particularly susceptible to corrosion in aqueous solutions. In an aqueous environment, it dissolves by an electrochemical reaction with water, resulting in the fast formation of soluble magnesium hydroxide ($Mg(OH)_2$ and the release of hydrogen according to Eq. 2 [1,3,7].

$$Mg + 2H_2O \rightarrow Mg(OH)_2 + H_2 \quad (2)$$

The corrosion resistance of magnesium alloys in aqueous solutions also depends strongly on the pH value. In alkaline solutions, the magnesium hydroxide layer forms a relatively stable surface film that protects the substrate from further attack [1,3]. In neutral or acidic environments, however, the magnesium hydroxide layer is not stable. In particular, in aqueous salt solutions the formed magnesium hydroxide film is removed very quickly and accelerates corrosion. Therefore, corrosion protection is very important for practical applications of components made of magnesium and its alloys [1,3,7,74].

The corrosion behavior of the uncoated and coated magnesium alloy AZ31 was investigated by immersing the samples in a 5 wt% NaCl solution for 168 h. Fig. 13 shows the surfaces of the uncoated magnesium substrate and the magnesium sample protected with the laser pyrolyzed Al_2O_3/ZrO_2-filled organosilazane based composite coating after the corrosion test.

As expected, the uncoated magnesium substrate showed pronounced

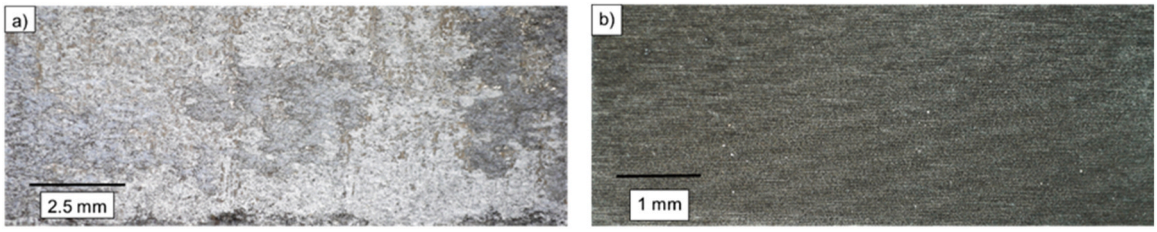

Fig. 13. Light microscope image of the surface after 168 h corrosion test in a 5 wt% NaCl solution, a) uncoated magnesium alloy, b) laser pyrolyzed Al_2O_3/ZrO_2-filled organosilazane based composite coating.

signs of corrosion after the test. According to Eq. 2, magnesium in contact with water initially forms a $Mg(OH)_2$ film, which is continuously dissolved by the chloride ions in the salt water, whereby the electrolyte comes again into contact with the unprotected magnesium substrate [1,3,73]. This causes continuous corrosion and decomposition of the magnesium substrate.

In contrast, no visible signs of corrosion were detected on the laser pyrolyzed coating. Especially pitting corrosion is a big problem of coated magnesium substrates in environments containing chloride ions. Such ions migrate through defects underneath the coating leading to coating failure through cracking and spalling [1,3,75]. As the laser pyrolysis formed a dense and chemically very stable ceramic layer, the magnesium substrate was well protected from corrosion also in saline environments.

In order to assess the corrosion mechanism more accurately, cross-sections of the uncoated magnesium alloy and of the laser pyrolyzed coating after the corrosion test were investigated by SEM and EDS (Fig. 14).

As already shown in Fig. 13, the cross-section and the associated EDS images of the uncoated magnesium alloy showed the formed porous Mg-O containing layer on the surface. XRD investigations, which are not discussed in detail, confirmed also the formation of magnesium hydroxide according to Eq. 2. The coated specimens showed no extensive signs of corrosion. The determined mass loss rate of the coated sample was $5.16 \bullet 10^{-4} \pm 0.10 \bullet 10^{-4}$ g/h•m^2, which was in relation to the uncoated substrate by a factor of about 1000 lower. In summary, the laser pyrolyzed coating exhibits excellent corrosion protection of the magnesium substrate.

3.2.5. *Thermal shock behavior*

Thermal stresses arise from inhomogeneous temperature distribution within coatings or by large differences in the coefficient of thermal expansion between a substrate and coating. Thereby ceramics predominantly fail at tensile stresses. The linear expansion coefficient (CTE) of the magnesium alloy is $23.5 \bullet 10^{-6}$ K^{-1}. The CTE of the coating components are $8.3 \bullet 10^{-6}$ K^{-1} for Al_2O_3 [41], $\approx 10.0 \bullet 10^{-6}$ K^{-1} for ZrO_2 [41] and $0.5 \bullet 10^{-6}$ K^{-1} for SiO_2 [76], which is formed during pyrolysis of the precursor. The values of the individual coating components are much lower than the CTE of the magnesium substrate. Therefore, tensile stresses occur within the coating during heating, which lead to cracks, delamination or spalling of the coatings if a critical stress value is exceeded.

To generate critical tensile stresses in the coating, the samples were first immersed in liquid nitrogen (-196 °C) and then immediately placed in an oven preheated to 400 °C for 15 min. This procedure was repeated five times.

Amazingly, after the thermal shock tests, the coating system showed neither spalling nor cracks at the interface to the magnesium substrate, indicating an excellent adhesion to the substrate (Fig. 15). The adhesion strength of the coating to the magnesium substrate after five thermal shock tests was 24.9 ± 1.4 MPa, which was approximately in the same range as before these tests (25.9 ± 2.7 MPa). These results indicate that the thermal tensile stresses generated during heating are lower than the adhesion strength of the coating. The coating hardness determined by nanoindentation measurements was 19.76 ± 2.31 GPa after the thermal shock test, which was also comparable to the value obtained directly after laser treatment of the coating (19.79 ± 1.90 GPa). Due to the constant high coating hardness, extensive micro crack formation within the coating as a result of the thermal shock tests can be excluded, since this would lead to an overall reduction of the coating hardness [41]. The high adhesion strength and coating hardness demonstrate that the coatings are also suitable for applications with high and multiple thermal stresses. The temperature gradient of almost 600 K used for the thermal shock tests was much higher than for common applications of magnesium.

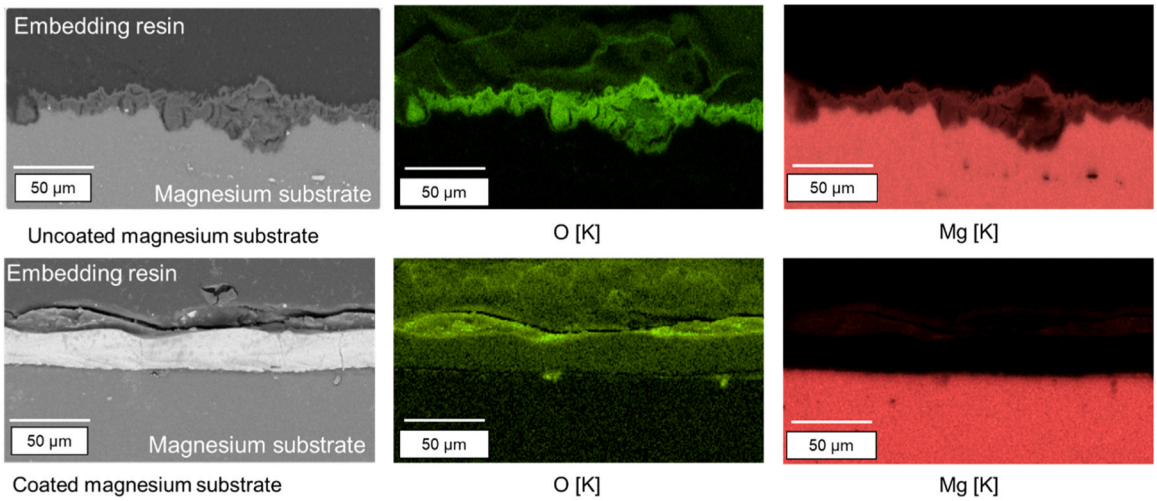

Fig. 14. SEM image with EDS-mappings of a cross section after 168 h test in 5 wt% NaCl solution of the uncoated and coated magnesium substrate.

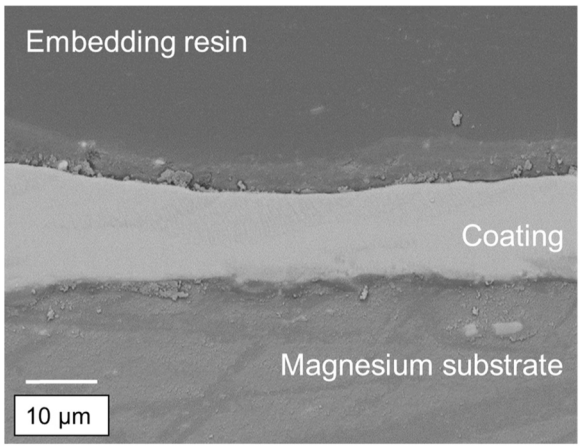

Fig. 15. SEM image of the laser pyrolyzed Al_2O_3/ZrO_2-filled organosilazane based composite coating after five thermal shock tests.

4. Conclusion

The present study reports about the Nd:YVO_4 laser based generation of fully ceramized Al_2O_3/ZrO_2-filled organosilazane based protective coatings on low-melting magnesium substrates. After melting of the alumina and zirconia fillers during the laser treatment, the subsequent solidification led to a planar and fine-grained structure in the vicinity of the magnesium substrate and a cellular/columnar-dendritic biphasic structure, composed of a ZrO_2-rich primary phase and Al_2O_3 enrichment between the ZrO_2 dendrites in the upper section of the coating. The coating was pore-free and dense without cracks at the interface to the substrate. Even the very high temperatures in the coating during laser treatment did not damage the substrate because of the high thermal conductivity of magnesium and the associated heat dissipation, the short interaction time between the laser beam and the coating as well as the very small ratio between the beam diameter and substrate volume.

The mechanical properties of the ceramic Al_2O_3/ZrO_2-filled organosilazane based coating system are outstanding. The hardness of the coating after laser treatment was 19.79 ± 1.90 GPa (HV 0.01), which is even higher or in a similar range as conventional coatings on magnesium produced via CVD and PVD. For comparison the hardness of the magnesium substrate is only 0.67 ± 0.01 GPa (HV 0.01). Also, the determined adhesive strength of 25.9 ± 2.7 MPa of the laser pyrolyzed coating on the magnesium substrate is very high and an important requirement for an effective wear protection. The sliding friction behavior of the ceramic coatings investigated by pin-on-disc method, was only 0.21 ± 0.02. This comparatively low value for ceramic surfaces effectively reduced wear caused by friction. In addition, the wear protection behavior of the coating was investigated by a method based on the linear Taber Abraser test using SiC-abrasive paper as counter body. While distinct wear marks and a large loss of material were detected on the uncoated magnesium substrate, no significant wear was observed on the coating. The ceramic coating is also characterized by an excellent corrosion protection of the magnesium substrate. The determined mass loss rate of the coated sample in relation to the uncoated substrate was reduced by a factor of about 1000, which makes the coating system very much suitable for corrosion protection applications. Despite huge differences in the CTE, the ceramic coating on the magnesium substrate exhibited superior thermal shock resistance. After multiple tests with a temperature gradient of almost 600 K, no ablation or defects were detected and neither the coating hardness nor the adhesion strength to the substrate changed after the tests.

In summary, the study demonstrates that the laser pyrolysis of the Al_2O_3/ZrO_2 filled organosilazane based coating system on a magnesium substrate led to dense, 20 µm thick, very well adhering ceramic coatings with a complex microstructure and excellent thermo-mechanical properties and chemical resistance. The laser process offers a flexible and low-cost method for the manufacturing of protective ceramic coatings on substrates with limited thermal resistance, low wear and corrosion resistance, which is not possible with other treatments.

CRediT authorship contribution statement

Alexander Horcher: Conceptualization, Data curation, Formal analysis, Investigation, Methodology, Validation, Writing – original draft. **Katja Tangermann-Gerk:** Conceptualization, Data curation, Formal analysis, Investigation, Methodology, Validation, Writing – original draft. **Walter Krenkel:** Formal analysis, Resources, Supervision, Validation. **Michael Schmidt:** Conceptualization, Funding acquisition, Methodology, Project administration, Resources, Writing – review & editing. **Stefan Schafföner:** Data curation, Formal analysis, Methodology, Resources, Supervision, Writing – review & editing. **Günter Motz:** Conceptualization, Formal analysis, Funding acquisition, Investigation, Methodology, Project administration, Supervision, Validation, Writing – review & editing.

Declaration of Competing Interest

The authors declare that they have no known competing financial interests or personal relationships that could have appeared to influence the work reported in this paper.

Data Availability

The raw/processed data required to reproduce these findings cannot be shared at this time as the data also forms part of an ongoing study.

Acknowledgments

The authors would like to thank DFG (Deutsche Forschungsgemeinschaft) for the financial support within the projects 405583003 (MO 851/19 and SCHM 2115/72).

References

[1] G.L. Makar, J. Kruger, Corrosion of magnesium, Int. Mater. Rev. 38 (1993) 138–153.
[2] H. Schreckenberger, Korrosion und Korrosionsschutz von Magnesium-Werkstoffen für den Automobilbau - Problematik der Kontaktkorrosion, VDI Verlag GmbH Düsseldorf, 2001.
[3] G.L. Song, A. Atrens, Corrosion mechanisms of magnesium alloys, Adv. Eng. Mater. 1 (1999) 11–33.
[4] K.U. Kainer. Magnesium. Eigenschaften, Anwendungen, Potenziale, 1st ed., Wiley-VCH, 2000.
[5] J.E. Gray, B. Luan, Protective coatings on magnesium and its alloys - A critical review, J. Alloy. Compd. 336 (2002) 88–113.
[6] J. Senf, E. Broszeit, Wear and corrosion protection of aluminum and magnesium alloys using chromium and chromium nitride PVD coatings, Adv. Eng. Mater. 1 (1999) 133–137.
[7] H.E. Friedrich, B.L. Mordike, Magnesium Technology, Springer-Verlag, Berlin, Heidelberg, 2006.
[8] K. Wang, M. Günthner, G. Motz, B.D. Flinn, R.K. Bordia, Control of surface energy of silicon oxynitride films, Langmuir 29 (2013) 2889–2896.
[9] M. Günthner, K. Wang, R.K. Bordia, G. Motz, Conversion behaviour and resulting mechanical properties of polysilazane-based coatings, J. Eur. Ceram. Soc. 32 (2012) 1883–1892.
[10] M. Günthner, T. Kraus, A. Dierdorf, D. Decker, W. Krenkel, G. Motz, Advanced coatings on the basis of Si(C)N precursors for protection of steel against oxidation, J. Eur. Ceram. Soc. 29 (2009) 2061–2068.
[11] M. Günthner, A. Schütz, U. Glatzel, K. Wang, R.K. Bordia, O. Greißl, W. Krenkel, G. Motz, High performance environmental barrier coatings, Part I: Passive filler loaded SiCN system for steel, J. Eur. Ceram. Soc. 31 (2011) 3003–3010.
[12] K. Wang, M. Günthner, G. Motz, R.K. Bordia, High performance environmental barrier coatings, Part II: Active filler loaded SiOC system for superalloys, J. Eur. Ceram. Soc. 31 (2011) 3011–3020.
[13] G. Barroso, T. Kraus, U. Degenhardt, M. Scheffler, G. Motz, Functional coatings based on preceramic polymers, Adv. Eng. Mater. 18 (2016) 746–753.
[14] J. Bill, F. Aldinger, Precursor-derived covalent ceramics, Precursor-Deriv. Ceram. Synth. Struct. High. Temp. Mech. Prop. (2007) 33–51.

[15] G. Barroso, Q. Li, R.K. Bordia, G. Motz, Polymeric and ceramic silicon-based coatings-a review, J. Mater. Chem. A 7 (2019) 1936–1963.
[16] P. Greil, Polymer derived engineering ceramics, Adv. Eng. Mater. 2 (2000) 339–348.
[17] P. Greil, Active-filler-controlled pyrolysis of preceramic polymers, J. Am. Ceram. Soc. 78 (1995) 835–848.
[18] H.-J. Bargel, G. Schulze. Werkstoffkunde, 11th ed., Springer, Heidelberg Dordrecht London New York, 2012.
[19] J. Wilden, G. Fischer, Laser synthesis of nanostructured ceramics from liquid precursors, Appl. Surf. Sci. 254 (2007) 1067–1072.
[20] A.P. Magee, P.R. Strutt, K.E. Gonsalves, Laser-induced conversion of molecular precursors to thin films and deposited layers, Chem. Mater. 2 (1990) 232–235.
[21] K.E. Gonsalves, P.R. Strutt, T.D. Xiao, P.G. Klemens, Synthesis of Si(C,N) nanoparticles by rapid laser polycondensation/crosslinking reactions of an organosilazane precursor, J. Mater. Sci. 27 (1992) 3231–3238.
[22] P. Colombo, A. Martucci, O. Fogato, P. Villoresi, Silicon carbide films by laser pyrolysis of polycarbosilane, J. Am. Ceram. Soc. 84 (2001) 224–226.
[23] H.-J. Krauß, Laserstrahlinduzierte Pyrolyse präkeramischer Polymere, Dissertation, Friedrich-Alexander-Universität Erlangen-Nürnberg, 2006.
[24] K. Tangermann-Gerk, G. Barroso, B. Weisenseel, P. Greil, T. Fey, M. Schmidt, G. Motz, Laser pyrolysis of an organosilazane-based glass/ZrO2 composite coating system, Mater. Des. 109 (2016) 644–651.
[25] A. Horcher, K. Tangermann-Gerk, G. Barroso, M. Schmidt, G. Motz, Laser and furnace pyrolyzed organosilazane-based glass/ZrO2 composite coating system—A comparison, J. Eur. Ceram. Soc. 40 (2020) 2642–2651.
[26] A. Horcher, K. Tangermann-Gerk, W. Krenkel, M. Schmidt, R.K. Bordia, G. Motz, Laser pyrolyzed organosilazane-based Al/ZrO2 composite coating on stainless steel: Resulting microstructure and mechanical properties, Int. J. Appl. Ceram. Technol. (2021) 1–10.
[27] Y. Cong, B. Li, S. Yue, D. Fan, X. Wang, Effect of oxygen vacancy on phase transition and photoluminescence properties of nanocrystalline zirconia synthesized by the one-pot reaction, J. Phys. Chem. C. 113 (2009) 13974–13978.
[28] G.A. Shafeev, Laser activation and metallisation of oxide ceramics, Adv. Mater. Opt. Electron. 2 (1993) 183–189.
[29] G.A. Shafeev, Laser activation and metallisation of insulators, Quantum Electron 27 (1997) 1104–1110.
[30] A. Horcher, K. Tangermann-Gerk, W. Krenkel, S. Schafföner, G. Motz, Advanced ceramic coatings on aluminum by laser treatment of filled organosilazane-based composites, Ceram. Int. 48 (2022) 23284–23292.
[31] M. von Allmen, A. Blatter, Laser-Beam Interactions with Materials, 2. Auflage, Springer-Verlag, Berlin, Heidelberg, 1995.
[32] C. Limmaneevichitr, S. Kou, Experiments to simulate effect of Marangoni convection on weld pool shape, Weld. J. -N. Y. 79.8 (2000) 231 (-s).
[33] D. Bäuerle, Laser Processing and Chemistry, Springer-Verlag Berlin Heidelberg, 2011.
[34] R. Poprawe, Lasertechnik für die Fertigung, Springer-Verlag Berlin Heidelberg, 2005.
[35] S. Trassl, G. Motz, E. Rössler, G. Ziegler, Characterization of the free-carbon phase in precursor-derived Si-C-N ceramics: I, spectroscopic methods, J. Am. Ceram. Soc. 85 (2002) 239–244.
[36] A. Müller, N. Herlin-Boime, F. Ténégal, X. Armand, F. Berger, A.M. Flank, R. Dez, K. Müller, J. Bill, F. Aldinger, Comparison of Si/C/N pre-ceramics obtained by laser pyrolysis or furnace thermolysis, J. Eur. Ceram. Soc. 23 (2003) 37–46.
[37] V.R. PaiVerneker, A.N. Petelin, F.J. Crowne, D.C. Nagle, Color-center-induced band-gap shift in yttria-stabilized zirconia, Phys. Rev. B 40 (1989) 8555–8557.
[38] G.A. Shafeev, Laser activation and metallisation of insulators, Quantum Electron 27 (1997) 1104–1110.
[39] W. Kurz, D.J. Fisher, Fundamentals of solidification, Trans Tech Publications Ltd., 1992.
[40] T. DebRoy, H.L. Wei, J.S. Zuback, T. Mukherjee, J.W. Elmer, J.O. Milewski, A. M. Beese, A. Wilson-Heid, A. De, W. Zhang, Additive manufacturing of metallic components – Process, structure and properties, Prog. Mater. Sci. 92 (2018) 112–224.
[41] H. Salmang, H. Scholze, Keramik, Springer-Verlag, Berlin Heidelberg, 2007.
[42] R. Chavez, E. Ionescu, C. Balan, C. Fasel, R. Riedel, Effect of ambient atmosphere on crosslinking of polysilazanes, J. Appl. Polym. Sci. 119 (2011) 794–802.
[43] G. Motz, T. Schmalz, S. Trassl, R. Kempe, Oxidation behavior of SiCN materials, in: Des. Process. Prop. Ceram. Mater. from Preceramic Precursors, Nova Science Publishers Inc, 2012, pp. 15–36.
[44] D. Bahloul, M. Pereira, P. Goursat, N.S.C.K. Yive, R.J.P. Corriu, Preparation of silicon carbonitrides from an organosilicon polymer: i, thermal decomposition of the crosslinked polysilazane, J. Am. Ceram. Soc. 76 (1993) 1156–1162.
[45] G. Gottstein. Materialwissenschaft und Werkstofftechnik, fourth ed., Springer-Verlag, Berlin, Heidelberg, 2014.
[46] T.F. Page, J.C. Knight, Factors affecting the tribological behavior of thin hard TiN and TiC coatings, Surf. Coat. Technol. 39- 40 (1989) 339–354.
[47] D. Amouzou, L. Fourdrinier, F. Maseri, R. Sporken, Formation of Me–O–Si covalent bonds at the interface between polysilazane and stainless steel, Appl. Surf. Sci. 320 (2014) 519–523.
[48] F. Czerwinski, Magnesium alloys – Corrosion and surface treatments, InTech, Rijeka, 2011.
[49] A. Krell, A new look at the influences of load, grain size and grain boundaries on the room temperature hardness of ceramics, Int. J. Refract. Met. Hard Mater. 16 (1998) 331–335.
[50] H. Altun, S. Sen, The effect of PVD coatings on the wear behaviour of magnesium alloys, Mater. Charact. 58 (2007) 917–921.
[51] F. Hollstein, R. Wiedemann, J. Scholz, Characteristics of PVD-coatings on AZ31hp magnesium alloys, Surf. Coat. Technol. 162 (2003) 261–268.
[52] T. Tański, K. Labisz, K. Lukaszkowicz, A. Śliwa, K. Gołombek, Characterisation and properties of hybrid coatings deposited onto magnesium alloys, Surf. Eng. 30 (2014) 927–932.
[53] T. Tański, Surface layers on the Mg-Al-Zn alloys coated using the CVD and PVD methods Manufacturing and processing, J. Achiev. Mater. Manuf. Eng. 53 (2012) 89–96.
[54] Y. Li Gao, C. Shan Wang, M. Yao, H. Bin Liu, The resistance to wear and corrosion of laser-cladding Al2O3 ceramic coating on Mg alloy, Appl. Surf. Sci. 253 (2007) 5306–5311.
[55] J.I. Wilkes, Selektives Laserschmelzen zur generativen Herstellung von Bauteilen aus hochfester Oxidkeramik, (2009).
[56] S.M. Lakiza, L.M. Lopato, Stable and Metastable Phase Relations in the System Alumina-Zirconia-Yttria, J. Am. Ceram. Soc. 80 (1997) 893–902.
[57] T.P. Hoepfner, E. Case, The influence of the microstructure on the hardness of sintered hydroxyapatite, Ceram. Int. 29 (2003) 699–706.
[58] J. Luo, R. Stevens, Porosity-dependence of elastic moduli and hardness of 3Y-TZP ceramics, Ceram. Int. 25 (1999) 281–286.
[59] R.M. German, S.J. Park, Handbook of mathematical relations in particulate materials processing, John Wiley & Sons, Inc, 2008.
[60] L. Wu, X. Guo, J. Zhang, Abrasive resistant coatings—a review, Lubricants 2 (2014) 66–89.
[61] D.M. Kennedy, M.S.J. Hashmi, Methods of wear testing for advanced surface coatings and bulk materials, J. Mater. Process. Technol. 77 (1998) 246–253.
[62] Y. Zhou, J. Peng, M. Wang, J. Mo, C. Deng, M. Zhu, Tribochemical behavior of pure magnesium during sliding friction, Metals 9 (2019).
[63] F.P. Bowden, D. Tabor, The Friction and Lubricants of Solids, Oxford University Press, 2001.
[64] E. Rabinowicz, Lubrication of metal surfaces by oxide films, Tribol. Trans. 10 (1967) 400–407.
[65] G. Bolelli, V. Cannillo, L. Lusvarghi, T. Manfredini, „Wear behaviour of thermally sprayed ceramic oxide coatings, Wear 261 (2006) 1298–1315.
[66] K. Kato, Wear in relation to friction — a review, Wear 241 (2000) 151–157.
[67] T. Cross, R. Raj, S.V. Prasad, T.E. Buchheit, D.R. Tallant, Mechanical and tribological behavior of polymer-derived ceramics constituted from $SiC_xO_yN_z$, J. Am. Ceram. Soc. 89 (2006) 3706–3714.
[68] D. Klaffke, Influence of counter body material and relative humidity on the tribological behavior of steel/ceramic couples. Proceedings, 2nd World Tribology Congress, Vienna, Austria, (2001).
[69] H. Czichos, Verschleiß, in: H. Czichos, K.-H. Habig (Eds.), Tribologie-Handbuch, 4. Auflage, Springer Vieweg, Wiesbaden, 2015.
[70] K. Sommer, R. Heinz, J. Schöfer, Verschleiß metallischer Werkstoffe, 3. Auflage, Springer Vieweg, Wiesbaden, 2018.
[71] M. Godet, The third-body approach: a mechanical view of wear, Wear 100 (1984) 437–452.
[72] M. Godet, Third-bodies in tribology, Wear 136 (1990) 29–45.
[73] E. Kunze, Korrosion und Korrosionsschutz, Wiley-VCH Verlag, 2001.
[74] A. Pardo, M.C. Merino, A.E. Coy, R. Arrabal, F. Viejo, E. Matykina, Corrosion behaviour of magnesium/aluminium alloys, Corros. Sci. 50 (2008) 823–834.
[75] P. Panjan, A. Drnovšek, P. Gselman, M. Čekada, Panjan, T. Bončina, D.K. Merl, Influence of growth defects on the corrosion resistance of sputter-deposited TiAlN hard coatings, Coatings 9 (2019).
[76] Manufacturer specifications Heraeus Quarzglas GmbH & Co. KG, 2021.